Heated Supersonic Axisymmetric Jet Cases for the NASA Turbulence Modeling Resource

Nicholas J. Georgiadis[1] and Vance F. Dippold, III[2]
NASA Glenn Research Center, Cleveland, OH 44135

Robert A. Baurle[3]
Air Force Research Laboratory, Wright-Patterson Air Force Base, OH 45433

Christopher L. Rumsey[4]
NASA Langley Research Center, *Hampton, VA 23681*

Three new supersonic jet cases were built for the NASA Turbulence Modeling Resource (TMR). These cases were taken from the 6th AIAA Propulsion Aerodynamics Workshop (PAW) nozzle test problem, which utilized data taken at NASA GRC consisting of non-intrusive measurements of jet plume velocities and temperatures, including both mean values and turbulence statistics. The three jet cases all used an axisymmetric nozzle designed to be perfectly expanded at Mach 1.63 run at the following conditions: (1) on-design, heated; (2) on-design, temperature-matched, and (3) overexpanded (off-design), heated. Computational fluid dynamics (CFD) solutions were obtained using three established Reynolds-averaged Navier-Stokes (RANS) codes: Wind-US, FUN3D, and VULCAN-CFD, all using the Menter Shear Stress Transport k-ω turbulence model with vorticity source term (SST-V). The NASA TMR requires at least two CFD codes yielding essentially identical results to certify that the approaches are verified, meaning that they solve the posed CFD equations as intended. The three codes generally provided very close agreement with each other for jet plume quantities, with the only exception being static temperature. This discrepancy was determined to be the result of whether or not turbulent kinetic energy was considered in the definition of total energy. Validation of the SST-V turbulence model for this case (its level of agreement/disagreement with experimental data) is also addressed.

Nomenclature

C_v	specific heat at constant volume
D	nozzle exit diameter = 50.8 mm =2.00 inches
E	total energy
k	turbulent kinetic energy
k_{rat}	ratio of turbulent kinetic energy, k, to U_{jet}^2
M	Mach number
M_a	acoustic Mach number
M_c	convective Mach number
M_{jet}	jet Mach number
NPR	nozzle pressure ratio = nozzle plenum total pressure / ambient static pressure
Pr_t	turbulent Prandtl number
r	radial coordinate
T	mean static temperature
T_{jet}	jet exit static temperature
T_t	jet stagnation temperature
T_∞	ambient static temperature
$\bar{u}, \bar{v}, \bar{w}$	mean velocities in cartesian coordinates
U_{jet}	jet exit velocity
$\overline{u'u'}, \overline{v'v'}, \overline{w'w'}$	turbulent normal stresses
$\overline{u'v'}$	turbulent shear stress

[1] Aerospace Engineer, Inlets and Nozzles Branch, Georgiadis@nasa.gov, AIAA Associate Fellow
[2] Aerospace Engineer, Inlets and Nozzles Branch, Vance.F.Dippold@nasa.gov, AIAA Senior Member
[3] Senior Technologist for Hypersonics, robert.baurle@us.af.mil, AIAA Associate Fellow
[4] Senior Research Scientist, Computational AeroSciences Branch, c.l.rumsey@nasa.gov, AIAA Fellow

x	axial coordinate
y	transverse coordinate
y+	wall coordinate
ΔT	difference between jet static temperature and ambient temperature, $T_{jet} - T_{\infty}$
ΔT_k	difference in calculated static temperature if including contribution of turbulent kinetic energy.
ω	specific turbulent dissipation rate

I. Introduction

The NASA Turbulence Modeling Resource[1-2] (TMR) is a website containing detailed information on Reynolds-averaged Navier-Stokes (RANS) turbulence models as well as several test cases intended to benchmark computational fluid dynamics (CFD) codes against experimental data, along with expected solutions using certified computational methods. Naturally, the first test cases constructed were canonical cases having relatively simple geometry flows at relatively low subsonic speeds. Over time, flow cases with varying aerodynamic challenges have been added. These cases include wall bounded flows at a range of Mach numbers up to supersonic speeds and free shear layer flows, including three subsonic jet cases. These subsonic jet cases all utilized convergent nozzles with plume measurements taken by Bridges and Wernet[3-4]. Two supersonic cases, measured against limited heated supersonic jet data of Seiner et al.[5], are also available. The experimental data available for these supersonic jet cases consists of centerline velocities and temperatures, measured with traditional stagnation temperature and pressure probes. The TMR cases for these Mach 2 jets have comparisons of CFD to experiment for calculations obtained with the Spalart-Allmaras one-equation turbulence model.[6] Numerous computational efforts have utilized this set of experimental data to evaluate Reynolds-averaged Navier-Stokes (RANS) CFD methods, with Refs. 7–11 as only a few examples. Several other efforts[12-16] have used the data to propose modifications to RANS methods for calculation of heated supersonic jets. Morris and Luke[17] modeled these experiments with implicit large eddy simulation (LES).

More recently, experimental data collected at NASA Glenn Research Center, Refs. 18-20, built upon the earlier Seiner experiments to use non-intrusive measurements of both velocities and temperatures for a series of supersonic jets. These newer experiments included Mach 2 jet cases to benchmark results against the earlier efforts of Seiner et al., and established close agreement with the former data collected using centerline total temperature and total pressure probe measurements. The newer data set was used in the 6th Propulsion Aerodynamics Workshop (PAW) sponsored by the American Institute of Aeronautics and Astronautics (AIAA) to investigate both RANS techniques as well as scale-resolving simulation (SRS) approaches. SRS directly computes turbulent structures in the focus region of a flow problem, which for supersonic jets is the jet plume mixing region. Results using RANS and SRS approaches obtained in the 6th PAW for the newer NASA GRC experiments are provided in Georgiadis et al.[21]

Supersonic jet flow fields have been studied extensively over the years, with interest in understanding and predicting jet plume mixing for purposes of acoustics, plume thermal impacts, and mixing characteristics. While round jets are relatively simple geometrically, the flow physics of heated supersonic jets have remained challenging for CFD methods to model accurately. The primary difficulties are accurately replicating the effects of turbulent thermal transport and reduced mixing rate due to compressibility. The objective of the 6th PAW nozzle test case was to assess the accuracy of existing CFD codes and modeling techniques in simulating the aerodynamics and thermodynamics of heated supersonic jet plumes from axisymmetric convergent-divergent (C-D) nozzles. Previous workshops focused on nozzle aerodynamics, propulsion efficiency, and heat transfer metrics.

This paper uses three of the cases utilized during the workshop to construct new axisymmetric jet cases for the NASA TMR. While these cases are categorized as validation cases on the TMR and do include comparisons with experimental measurement, the initial intent was to create verification cases, or in other words cases intending to ensure that the computational models (in terms of equations solved) have been correctly replicated as intended, and that mesh independent results are achieved. The results of three NASA codes applied to the three jet cases are compared to each other and experimental data.

II. Nozzle/Jet Case Details

A. Nozzle Experimental Configuration:

In the 6th AIAA PAW, three axisymmetric convergent-divergent nozzles, designed using the method of characteristics to provide as close to a uniform nozzle exit flow free of shock waves as possible, were investigated. The nozzles were designed to provide Mach 1.36, 1.63, and 2.00 perfectly expanded flows at the nozzle exit, and all three had the same exit diameter, D = 50.8 mm (2.00 inches). For the TMR cases discussed here, only the Mach 1.63

nozzle was used, with three operating points selected as shown in Table 1. The case number shown in the first column table refers to the case number designation from the PAW workshop.

In the experiments, the nozzle was operated by controlling the supply of total pressure to achieve the jet exit Mach number (M_{jet}) corresponding to a given nozzle pressure ratio (NPR = supply total pressure / ambient static pressure) and nozzle static temperature difference (ΔT = calculated jet exit static temperature - ambient static temperature). It is standard in many aerodynamic CFD simulations to assume a calorically perfect gas, such that the specific heat ratio, γ, is constant, and if the working fluid is air, $\gamma = 1.4$. The NPR and calculated jet Mach number, M_{jet} shown in Table 1 assumes $\gamma = 1.4$. In the experiments, hydrogen was combusted to heat the air to the desired temperature. The primary effect of H_2O in the exhaust gas was to slightly reduce the nozzle flow rate and to minimally change the gas properties. For the calculations to be obtained for these cases, clean air with $\gamma = 1.4$ was simulated, and employing a variable γ capability or accounting for H_2O would not be expected to change the results significantly.

Table 1. Operating Conditions

PAW6 Case	Nozzle Geometry Mach No.	Nozzle Operating Mach No.	NPR	Nozzle T_t (K)	Jet ΔT (K) = $T_{jet} - T_\infty$	U_{jet} (m/s)	M_c	M_a
5	1.63	1.63	4.44	442.1	0	555.2	0.68	1.36
2	1.63	1.63	4.44	799.4	233	746.6	0.93	2.19
4	1.63	1.36	3.01	715.2	233	594.0*	0.78	1.83

**U_{jet} based on supply conditions would be 622.9 m/s but as discussed in the Results section, a normal shock reduces the effective U_{jet} to 594.0 m/s.*

The convective Mach number (M_c) shown in Table 1, as defined in Eqn. 1, is a measure of the compressibility of the jet. The acoustic Mach number (M_a), as defined in Eqn. 2, is used in the jet aeroacoustics community to relate the jet exhaust speed to the ambient air speed of sound and hence characterize the propagation of jet mixing noise. Bridges and Wernet[3-4] employed M_a to assemble the matrix of convergent nozzle jets in their experiments. A nearly sonic heated jet can have $M_{jet} < 1$ but $M_a > 1$. Also note that for a temperature matched jet, such as PAW Case 5 in Table 1, $T_{jet} = T_\infty$, $M_a = 2\, M_c$.

$$M_c = U_{jet} / (\sqrt{\gamma R T_{jet}} + \sqrt{\gamma R T_\infty}) \quad (1)$$

$$M_a = U_{jet} / \sqrt{\gamma R T_\infty} \quad (2)$$

During the tests, the freestream conditions varied from day-to-day and even during a single day's testing, but for the purposes of CFD investigations, Ref. 21 recommended using a constant assumed static pressure of 99.28 kPA (14.4 psi) and static temperature of 288.9 K (520 R) for the ambient conditions. These were reference ambient properties used to calculate the ideal jet exit velocities shown in Table 1.

The first case in the table (PAW Case 5) is for the Mach 1.63 nozzle, with on-design pressure ratio and has ΔT = 0 K, or in other words, no static temperature difference between the nozzle exhaust and the ambient air at the nozzle exit. The second case (PAW Case 2) shown in Table 1 represents on-design Mach 1.63 nozzle flow with jet exit ΔT = 233 K. The third case in the table (PAW Case 4) examines an off-design, overexpanded case where the Mach 1.63 nozzle is run at heated flow supply conditions identical to that for a Mach 1.36 nozzle. In other words, the NPR of this case is lower than that required to achieve a fully expanded state at the nozzle exit for the Mach 1.63 nozzle contour.

B. Computational Grids:

A set of computational grids were developed for the PAW and used here for the TMR cases with a RANS structured topology using the Pointwise[22] software to create meshes for the axisymmetric geometry, with the axis of the nozzle and jet serving as the bottom of the grid. A view of the computational grid constructed for the Mach 1.63 nozzle is shown in Fig. 1. The internal geometry of the experimental test article is reproduced as far upstream as the supply pipe. The geometry of the outside of the nozzle, adapter, and supply pipe is also modeled very closely with the exception that in this axisymmetric representation, the regions of the external surface locations where fasteners were used to attach the components of the assembly were faired over. As the nozzle experiments were run with zero

co-flow, this change is not expected to be a significant modeling deviation. The lip thickness at the exit plane of the nozzle is 0.76 mm.

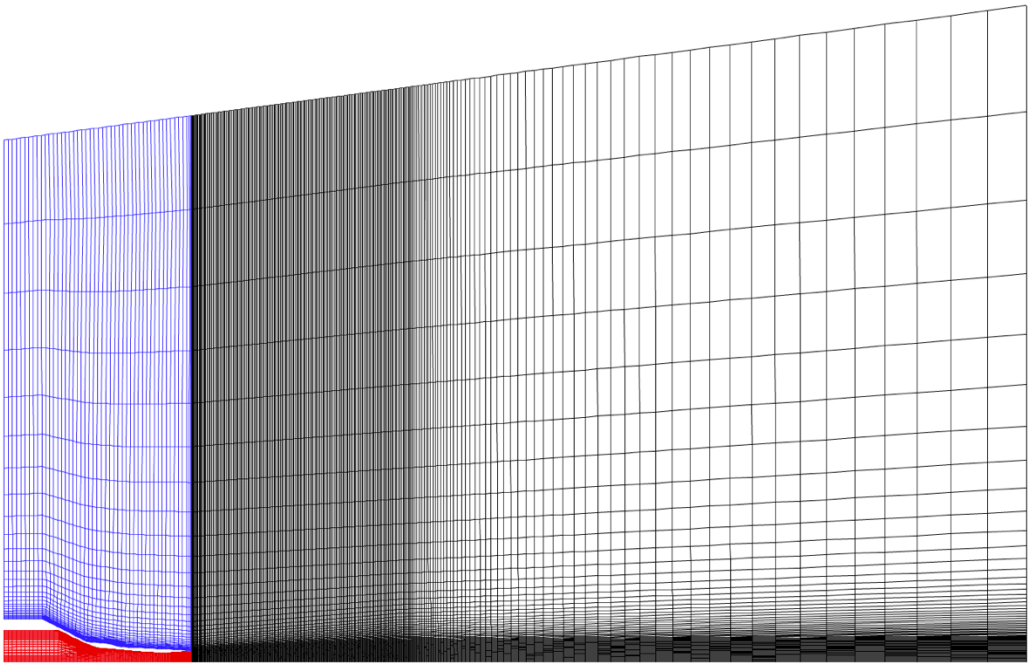

(a) Entire grid

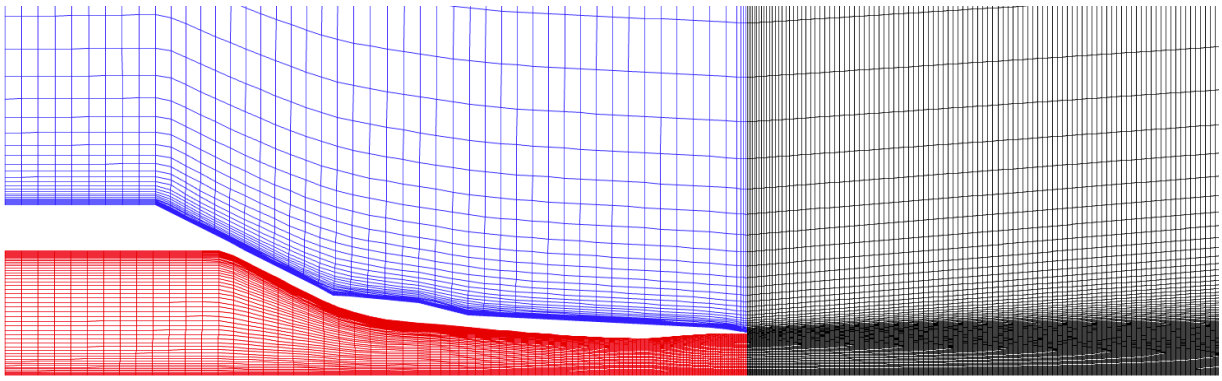

(b) Detail near nozzle exit

Fig. 1.—Computational grid for Mach 1.63 nozzle (every 4th point shown in the axial and radial directions for clarity).

Using the structured grid approach, three zones were utilized with point-to-point matching at zonal interfaces. The location of the axis of symmetry at the nozzle exit is set as the origin of the computational domain (i.e. x,r = 0,0). The three zones were comprised of: (1) nozzle internal region (401 axial points by 281 radial points), (2) external nozzle region and extending radially (201 by 161 points), (3) the jet plume region (961 by 481 points). All of these grid counts are for the finest level. The nozzle lip has 41 points. The axial spacing of the grid at the nozzle exit was 0.005D, and the grids extended 40D to the outflow boundary. Radially, the second zone has an inflow plane that extends 25D away from the centerline. The farfield boundary has a 7.5 degree divergence angle, starting from zone 2 and extending into zone 3, to ensure that any entrained ambient air enters the flow domain. As a result, at the jet plume zone outflow station (at x/D = 40) in zone 3, the farfield boundary extends to 32.45D.

The supplied structured grids may be coarsened to study RANS solver grid convergence following the philosophy of cases available on the NASA Turbulence Modeling Resource[1-2]. These grids may be sequenced (i.e. agglomerated

by removing every other point) in each direction 3 times to provide 4 grid sets with: (1) un-sequenced: 401 × 281, 201 × 161, 961 × 481, (2) 1-level sequenced: 201 × 141, 101 × 81, 481 × 241, (3) 2-level sequenced: 101 × 71, 51 × 41, 241 × 121, (4) 3-level sequenced: 51 × 36, 26 × 21, 121 × 61.

The grid was packed to the nozzle wall at $\Delta y = 0.00005D$, such that the nominal y+ of the first point off the wall in the supersonic portion of the nozzle was on the order of 1 on the finest grid. With only entrained slow flow outside the nozzle, the wall spacing on the external portion of the nozzle was packed much less tightly, $\Delta y = 0.001D$.

Note that these computational grids were built and checkout runs were conducted using CFD strategies very similar to the three test cases available via the NASA turbulence modeling resource (turbmodels.larc.nasa.gov), namely the "Axisymmetric Subsonic Jet," "Axisymmetric Hot Subsonic Jet," and "Axisymmetric Near-sonic Jet" cases. The three-zone approach and overall gridding strategies were similar to the grids discussed here for the supersonic jet cases, although finer grid resolution in the potential core region was used here for the supersonic cases, especially needed for the off-design case with shock waves in the jet plume. In the PAW, it was found that solutions obtained with the two finest grids were nearly indistinguishable using several two-equation RANS turbulence models and even the 2-level sequenced grids provided results that were very close to the two finer levels, as shown in Ref. 21. The results reported here were obtained using the finest grid.

C. Boundary Conditions and Flow Solver Settings:

The boundary conditions required to run these nozzle cases are relatively straightforward, at least for a steady RANS approach. The stagnation pressure and temperature for each case may be obtained from Table 1 and applied at the inflow to the nozzle. In the experiments, there was no external co-flow, but some forward velocity needs to be prescribed with most CFD solvers to enable convergence. Preliminary test calculations were performed for the grids discussed in the previous section with multiple flow solvers utilizing a freestream condition set to Mach 0.01. It is generally desirable to set this freestream Mach number as low as possible but increasing it as high as Mach 0.05 did not affect the jet solutions significantly for this case. On the finest grid level, many general purpose RANS solvers have difficulty obtaining converged steady-state solutions with a constant CFL solver approach. Completing these solutions with a time-accurate (constant time step) approach is frequently required, as was the case in the current investigation, to obtain a thoroughly converged RANS solution. As suggested previously, a constant assumed static pressure of 99.28 kPA (14.4 psi) and static temperature of 288.9 K (520 R) were used for the ambient conditions in these simulation cases.

It is believed that the flows inside the nozzles generated turbulent boundary layers, although measurements were not made inside the nozzle to verify this. Heat transfer to the nozzle structure was not expected to be a significant factor, so adiabatic wall boundary conditions were set for the interior and exterior surfaces of the nozzle. Zore et al.[23] participated in the PAW and conducted a conjugate heat transfer analysis that verified heat transfer did not significantly affect the internal nozzle boundary layers nor jet plumes. The nozzle structure was constructed from 316 stainless steel which does not have a high thermal conductivity. The default turbulent Prandtl number (Pr_t) used in most production CFD codes is 0.9 but there are some studies[24] which have indicated that using $Pr_t = 0.7$ may be more accurate for jet flows. All of the codes utilized $Pr_t = 0.9$ for the cases investigated here.

D. Approaches Utilized

Three widely used RANS-based solvers were used for the preliminary investigations discussed in this paper: Wind-US[25], FUN3D[26], and VULCAN-CFD[27]. For the baseline results shown in this paper, all codes employed the Shear Stress Transport (SST) k-ω model of Menter[28-29] using a vorticity-based production term for the turbulent kinetic energy. On the NASA TMR, this form of the model is referred to as either SST-V or SST-Vm, depending on whether the $2/3\rho k\delta_{ij}$ term is ignored in the production term and the momentum and energy equations. Because this term only affects normal stresses and the jet problems under examination are dominated by shear forces, the SST-V or SST-Vm yield nearly identical results for these axisymmetric jets, and hereafter we refer to the modeling as SST-V. After these cases are established on the TMR website, it is expected that additional turbulence models will be added, but the results here utilize the SST-V two-equation model because it has been one of the most widely used RANS models for jet flows. Wind-US and VULCAN-CFD utilized structured flow solvers and FUN3D utilized an unstructured flow solver, and all used the workshop provided structured meshes.

III. Results

A. Temperature-Matched Mach 1.63 Axisymmetric Jet:

The temperature matched case was set experimentally by heating the nozzle plenum flow to a total temperature, that when expanded through the convergent-divergent nozzle to a Mach 1.63 exit state, yielded a static temperature

that matched ambient and hence provided no mean thermal gradient. A comparison of computational solutions obtained with the three CFD codes is made with experimental data for centerline velocities and turbulent kinetic energy in Figs. 2-3. As expected, the RANS solutions overpredict mixing rate for these supersonic jets. Compressibility effects, which have been observed to reduce the mixing rate relative to incompressible jets, are not captured accurately by the standard (uncorrected) two-equation turbulence models. Recall, however, the purpose of these TMR cases is not detailed scrutiny of the performance of the RANS modeling, but rather establishing the expected benchmark results for a given RANS turbulence model.

The mean velocities shown in Fig. 2 and turbulent kinetic energy results shown in Fig. 3 demonstrate that all of the solutions predict higher centerline turbulent kinetic energy levels than those measured experimentally. The experimental streamwise PIV data used to compare to the computational results did not measure $\overline{w'w'}$, but Ref. 19 showed that it can be reasonably approximated as $\frac{3}{2}\overline{v'v'}$, and k can be approximated as shown in Eqn. 3.

$$k = \frac{1}{2}(\overline{u'u'} + \overline{v'v'} + \overline{w'w'}) \approx \frac{1}{2}\left(\overline{u'u'} + \overline{v'v'} + \frac{3}{2}\overline{v'v'}\right) = \frac{1}{2}\overline{u'u'} + \frac{5}{4}\overline{v'v'} \tag{3}$$

All of the RANS solutions exhibit essentially no centerline turbulent kinetic energy until an axial location corresponding to the end of the potential core. Then there is an abrupt rise in turbulent kinetic energy levels near x/D = 8. In contrast, the experimental data exhibits a more gradual initial increase in turbulent kinetic energy levels that initiates before the end of the potential core, around $x/D = 5$. The actual jet has a potential core length that instantaneously varies in time and as a result there is intermittent turbulence. This upstream turbulence arises from the portion of time when the jet potential core is shorter than the mean potential core length. The RANS solutions, which by design are only representing a time averaged solution, are generally unable to replicate this intermittent turbulence appearing before the end of the mean jet potential core, starting at about $x/D = 5$.

Profiles of axial velocity, turbulent kinetic energy, and turbulent shear stress are provided in Fig. 4 at several axial stations in the jet plume. Close agreement is observed between the three codes for all quantities, although the discrepancy of the solutions with experimental data is readily apparent. The close agreement of the three flow solvers establishes that the same modeling approach in independent flow solvers should be expected to yield similar results of jet flow predictions.

B. Heated Mach 1.63 Axisymmetric Jet:

The comparison of centerline velocities and turbulent kinetic energy for the heated case, shown in Figs. 5-6, show similar agreement to that for the unheated case in the previous section. However, when using the default output from the three RANS codes for temperatures (Fig. 7), it was noted that the VULCAN-CFD result was substantially different than that from the other two codes. It was found that the form of the total energy equation solved by VULCAN-CFD differed from that of Wind-US and FUN3D, in that VULCAN-CFD included the turbulent kinetic energy, while the other two codes ignored this contribution to the total energy.

In compressible flow problems, the energy equation contains extra terms from the time-averaging process that are typically ignored in incompressible or low Mach number situations. These terms are the molecular diffusion and turbulent transport of turbulent kinetic energy. For the jet flow problems considered here, contributions of these terms remain small. The derivation of these terms, using Favre averaging, is described in detail on the page Implementing Turbulence Models into the Compressible RANS Equations on the TMR and also in Wilcox.[30] The total energy also has a contribution from turbulent kinetic energy, k, which may not be significant for subsonic flows or where the turbulent kinetic energy is a small fraction of the mean kinetic energy:

$$E = C_v T + \frac{1}{2}(\bar{u}^2 + \bar{v}^2 + \bar{w}^2) + k \tag{4}$$

However, for these jet flows, k is a non-trivial component of the overall energy. The default solution procedures for two of the codes used to obtain results here (and used typically for lower speed flow analyses), FUN3D and Wind-US, do not consider the contribution of k in the total energy expression. It is noted that an alternate formulation available in FUN3D intended for non-calorically perfect gas, high Mach number applications does include this more complete form of the total energy term. The default procedure in VULCAN-CFD does include contribution of k in the total energy expression. Examining the centerline comparisons first, it may be observed that the centerline mean velocities and k show very close agreement with each other, regardless of treatment of k in the total energy equation. The centerline static temperature comparisons, however, show a significant effect of this treatment. The default solution procedure of the three codes, shown by solid lines, shows close agreement between FUN3D and Wind-US,

but not VULCAN-CFD. When we take this VULCAN-CFD solution and as a simple post-processing step add k back into the expression for temperature derived from Eq. 4, thus yielding a result that ignores the contribution of k in E, we arrive at centerline temperatures that are in close agreement with the two other codes; this is shown by the dashed black line, denoted as "VULCAN-CFD w/o k in E". This is essentially the same as never having subtracted out k from E when computing T.

Further comparisons of profiles at several axial stations exhibit the same trends, as shown in Figs. 8 and 9. The mean velocity, turbulent kinetic energy, and turbulent shear stress of the three codes are very similar and hence unaffected by the assumption of whether or not to include the turbulent kinetic energy in the total energy equation. The static temperatures, however, differ depending on how the turbulent kinetic energy is handled in the total energy budget. The default solutions from the three codes yield profiles in the first temperature profile plots (with all solid lines), which show VULCAN-CFD differing from FUN3D and Wind-US. The second temperature profiles plot, with the VULCAN-CFD solution essentially ignoring the contribution of k in E (shown with a dashed line and denoted as "VULCAN-CFD w/o k in E") results in very close agreement with solutions from the other two codes. The conclusion should not be drawn that the CFD solutions ignoring k in E are more accurate than solutions in which k is subtracted from E before computing temperature (the default VULCAN-CFD result) simply because the former lines are closer to the experimental data points for this particular case.

To examine the contribution of k in the energy equation, we must compare k with the internal energy, C_vT. The net change in calculated static temperature at every point in the flow is $\Delta T_k = k(\gamma-1)/R$. Examining Fig. 8(b), the ratio of k to U_{jet}^2, k_{rat}, reaches a peak value nearly equal to 0.03 in the current RANS simulations. Using $U_{jet}^2 = \gamma RT_{jet}M_{jet}^2$, the ratio of turbulent kinetic energy to the internal energy may be written as:

$$k/C_vT \cong \left[k_{rat}\gamma RT_{jet}M_{jet}^2\right]/[RT/(\gamma-1)] = k_{rat}\gamma(\gamma-1)M_{jet}^2\,T_{jet}/T \tag{5}$$

For the Mach 1.63 jets examined here, the peak value of the energy ratio is $k/C_vT \cong .045\,T_{jet}/T$. Similarly the peak value of ΔT_k can be written as follows:

$$\Delta T_k = k(\gamma-1)/R \cong k_{rat}\gamma(\gamma-1)M_{jet}^2T_{jet} \tag{6}$$

With our choice of normalizing jet temperatures by ΔT, the difference between jet static temperature and ambient temperature, $T_{jet} - T_\infty$, $\Delta T_k / \Delta T$ reaches a peak value of 10 percent in the shear layer for this case.

The key take-away exhibited by these jet results is that ignoring the contribution of turbulent kinetic energy in the total energy may not be an accurate assumption for flows at Mach numbers higher than unity, and especially where the turbulent transport of heat is important to the analysis. A similar result is evident for the **Off-Design Mach 1.63 Axisymmetric Jet** discussed in the next section.

C. Off-Design Mach 1.63 Axisymmetric Jet:

A comparison of centerline velocities for the off-design case is shown in Fig. 10. Computations of this off-design case showed that there is a normal shock of the overexpanded flow near the nozzle exit that extends a small distance away from the centerline. This normal shock locally reduces the stagnation pressure, such that the effective U_{jet} = 594.0 m/s, which is lower than the value which would be expected (622.9 m/s) if the nozzle supply air had been isentropically expanded to the ambient pressure. This value is used to normalize the off-design case velocities and turbulent stresses in Fig. 8 and subsequent plots for the off-design case. It may be observed that all three codes are able to replicate the experimentally measured centerline velocities in the oblique shock train of the overexpanded jet. In order to provide this agreement, the computational grid has to be fine enough not only in the direction normal to the jet flow direction but also axially. At the finest grid level, the plume zone has 700 axial points for $0<x/D<10$, starting with 0.25 mm spacing, and constant spacing (0.75 mm) from $1<x/D<10$. Frequently, a RANS jet plume grid is stretched continuously proceeding from the nozzle exit. Doing so for this jet case with shocks would result in attenuation of the shock reflections near the end of the potential core. It may be noted that downstream of the potential core and all of the shock reflections, the agreement of the computational solutions with experimental data is better than for the other two cases discussed in this report without shocks. This is not the result of more accurately capturing the flow physics of this case, but rather a fortuitous result of the effective jet Mach number in the potential core being substantially lower than the Mach 1.63 design of the nozzle, and hence yielding reduced compressibility effects in the jet that the computations are not accounting for.

The turbulent kinetic energy along the centerline, as shown in Fig. 11, once again shows that the computations fortuitously match the experimental data better than the computations for the other two supersonic jet cases discussed

earlier in this report. Upstream, experimental data shows a much earlier rise in centerline "turbulence" than the other cases. The individual rms velocity components that are used to calculate k also show evidence of the oscillations, although what is being calculated as turbulence intensity is more due to unsteady shock motion rather than vortical turbulence. The RANS calculations, which by design converge on a single steady state solution, have no ability to replicate this early centerline behavior and instead show a delayed and more abrupt rise in centerline turbulent kinetic energy.

The centerline static temperatures exhibit close agreement between the three computational solutions and experimental data, as shown in Fig. 12. At the end of the potential core and downstream, however, similar disagreement between the baseline VULCAN-CFD result and those from the other two codes is evident, as was the case for the on-design heated Mach 1.63 jet case. The modified VULCAN-CFD result, which more closely matches the two-equation model implementation in the other two codes, provides a closer match to the temperature obtained from the other two codes. Mean velocity, turbulent kinetic energy (k), and turbulent shear stress comparisons are shown in Fig. 13 with results showing little effect on whether k is accounted for in the total energy. Two sets of temperature profiles are shown in Fig. 14, the first with the standard VULCAN-CFD result showing small differences with the other two codes and the second with the VULCAN-CFD result postprocessed to yield an effective temperature calculated without consideration of k in E yielding closer agreement with the FUN3D and Wind-US results.

D. Assessment of RANS Modeling Trends for Jet Compressibility and Heating:

While the primary purpose of these three new supersonic jet cases for the TMR is to establish verified benchmark results for a given turbulence model using three widely used RANS solvers, we may use the results for these cases to make an assessment of linear two-equation RANS modeling in capturing the trends of jet compressibility and heating effects. Or in other words, we may validate the chosen RANS approach by assessing its ability to differentiate supersonic jet mixing (with and without heating) with well-established mixing behavior from low subsonic and unheated conditions. As mentioned in the introduction, there are subsonic cases available on the TMR for convergent nozzles with the same exit diameter, measured with the same PIV technique, and also measured in the same facility. The first subsonic jet case, known as the "Axisymmetric Subsonic Jet", was unheated and $M_{jet} = 0.50$. The second subsonic case, known as the "Axisymmetric Hot Subsonic Jet", has an exit velocity equal to that of the unheated jet but with a higher jet exit temperature ($M_{jet} = 0.38$). For the unheated case, the jet is treated as having $\Delta T = 0$ K, while for the heated case, $\Delta T = 225$ K. We consider both jet Mach numbers to be low enough to be considered effectively incompressible, and the differences in ΔT are close to the two on design supersonic jets considered in this report ($\Delta T = 0$ K and $\Delta T = 233$ K).

In Fig. 15, we compare the subsonic and supersonic jet centerline velocities and turbulent kinetic energy for experimental data and computational solutions obtained with the Wind-US code and SST-V. First examining the experimental data, we may observe that when holding ΔT constant, there is a definitive lengthening of the potential core and reduced downstream mixing rate that occurs due to compressibility effects from increasing the jet Mach number from low subsonic to Mach 1.63. Examining the computational solutions for either pair of subsonic/supersonic jets, the RANS method employed here is shown to have no ability to replicate compressibility effects. In contrast to the supersonic jet results discussed earlier in this paper, standard RANS with linear two-equation turbulence modeling and conventional closure coefficients yields potential cores that are too long in comparison with experimental data for low subsonic speed jets, but then downstream mixing that is much too fast relative to experiment. In terms of heating effects while holding the jet exit Mach number relatively constant, the experimental results show that heating tends to result in a shorter potential core length. This general trend is replicated qualitatively with the RANS computations.

A detailed interrogation of the RANS method applied to jets, and consideration of corrections that may more effectively capture some of these differences between subsonic and supersonic jets (empirical as they may be), is beyond the scope of this paper, and we refer the reader to the PAW summary paper[21] or the other references discussed in the introduction. Many attempts over several decades to produce a general RANS model to capture the effects of jet compressibility and heating effects have failed to yield a physics-based model that can serve as a broadly accurate computational prediction tool. If future RANS modeling improvements are developed, it is hoped that the test cases established here can be utilized to readily demonstrate the improvements over existing general purpose RANS models.

IV. Conclusions

This paper provides comparisons of three established RANS solvers for three new supersonic heated jet cases for the NASA Turbulence Modeling Resource (TMR) using the Menter SST-V k-ω turbulence model. The three jet cases are referred to as **"Temperature-Matched Mach 1.63 Axisymmetric Jet," "Heated Mach 1.63 Axisymmetric**

Jet," and **"Off-Design Mach 1.63 Axisymmetric Jet."** The first case was selected as a case with compressibility effects reducing the turbulent mixing, with no difference in mean temperature of the jet exiting the nozzle and that of the ambient, and hence did not include jet heating effects. The second case, with a significant difference between the jet static temperature and that of the ambient, was selected to investigate effects of both compressibility and heating. The third case was for a heated supersonic jet run at a pressure ratio that would produce an off-design overexpanded jet with a shock train in the potential core.

Results show very close agreement of the three codes in terms of axial velocities and turbulent statistics for all three cases when using the same grid, similar code settings, and the same turbulence model. The heated jet case is the first from the TMR to directly compare with in-flow measured temperatures. Through comparison with this temperature data, it was found that the default treatment for turbulent kinetic energy in the total energy equation solved by these three codes differed, which resulted in noticeable differences in predicted jet temperatures. For the off-design case, the computations showed good agreement for the mean velocity and temperature oscillations in the potential core having an oblique shock train.

The primary purpose of these new supersonic jet cases on the NASA TMR is to demonstrate that multiple codes can produce the same result for a given turbulence model implementation. Documenting the shortcomings of the model compared with experiment is then possible. Only one turbulence model was examined here, namely the Menter Shear Stress Transport (SST) k-ω turbulence formulation with vorticity source term (SST-V). Examination of other RANS turbulence models by other contributors would be welcome, provided the results were verified through computations with more than one established CFD code. With large-eddy simulation (LES) becoming the preferred CFD choice for higher accuracy jet physics modeling, perhaps this baseline using standard RANS modeling can be used to show the advantages of scale-resolving methods over RANS methods, which may be much less computationally expensive than LES, but limited in ability to replicate the effects of heated compressible round jets.

The links for all of the cases, with computational grids, experimental data, and sample computational results as documented in this report are as shown below:

AJM163TM: Temperature-Matched Mach 1.63 Axisymmetric Jet:
https://turbmodels.larc.nasa.gov/jet_mach1p63_tmatched_val.html
AJM163H: Heated Mach 1.63 Axisymmetric Jet:
https://turbmodels.larc.nasa.gov/jet_mach1p63_hot_val.html
AJM163OD: Off-Design Mach 1.63 Axisymmetric Jet:
https://turbmodels.larc.nasa.gov/jet_mach1p63_offdesign_val.html

Acknowledgments

This work of the authors was supported by the Transformational Tools and Technologies (TTT) Project of NASA's Transformative Aeronautics Concepts Program (TACP) and Hypersonic Technology Project (HTP) of the Advanced Air Vehicle Program (AAVP).

References

1. Rumsey, C., Smith, B., and Huang, G., "Description of a Website Resource for Turbulence Modeling Verification and Validation," AIAA Paper 2010-4742, June 2010.
2. Rumsey, C. L., "Recent Developments on the Turbulence Modeling Resource Website (Invited)," AIAA Paper 2015-2927, June 2015.
3. Bridges, J. and Wernet, M. P., "Establishing Consensus Turbulence Statistics for Hot Subsonic Jets," AIAA Paper 2010-3751, June 2010.
4. Bridges, J. and Wernet, M. P., "The NASA Subsonic Jet Particle Image Velocimetry (PIV) Dataset," NASA-TM 2011-216807, Nov. 2011.
5. Seiner, J. M., Ponton, M. K., Jansen, B. J., and Lagen, N. T., "The Effect of Temperature on Jet Noise Emission," AIAA Paper 92-02-046, 1992.
6. Spalart, P. R. and Allmaras, S. R., "A One-Equation Turbulence Model for Aerodynamic Flows," *La Recherche Aerospatiale,* Vol. 1, 1994, pp. 5-21.
7. Abdol-Hamid, K. S., Carlson, J. R., and Rumsey, C. L., "Verification and Validation of the k-kL Turbulence Model in FUN3D and CFL3D," AIAA Paper 2016–3941, Jan. 2016.
8. Yoder, D. A., Georgiadis, N. J., and O'Gara, M. R., "Frozen Chemistry Effects on Nozzle Performance Simulations," AIAA Paper 2008-3969, Jan. 2008.
9. Dembowski, M. A. and Georgiadis, N. J., "An Evaluation of Parameters Influencing Jet Mixing Using the WIND Navier-Stokes Code," NASA TM 2002-211727, Aug. 2002.

10. Barber, T. J., Chiapetta, L. M., DeBonis, J. R., Georgiadis, N. J., and Yoder, D. A., "Assessment of Parameters Influencing the Prediction of Shear Layer Mixing," *Journal of Propulsion and Power*, Vol. 15, No. 1, 1998, pp. 45–53.
11. Georgiadis, N.J., Yoder, D.A., Vyas, M.A., and Engblom, W.A., "Status of Turbulence Modeling for Hypersonic Propulsion Flowpaths," *Theor. Comput. Fluid Dyn*., Vol. 28, 2014, pp. 295-318.
12. Papp, J. and Dash, S., "Turbulence Model Unification and Assessment for High-Speed Aeropropulsive Flows," AIAA Paper 2001–0880, Jan. 2001.
13. Papp, J., Kenzakowski, D., and Dash, S., "Calibration and Validation of EASM Turbulence Model Jet Flowfields," AIAA Paper 2002–0855, Jan. 2002.
14. Tam, C. K. W. and Thies, A. T., "Computation of Turbulent Axisymmetric and Nonaxisymmetric Jet Flows Using the k-ϵ Model," *AIAA Journal*, Vol. 34, No. 2, Feb. 1996, pp. 309–316.
15. Tam, C. K. W. and Ganesan, A., "A Modified k-ε Turbulence Model for Calculating the Hot Jet Mean Flows and Noise," *AIAA Journal*, Vol. 42, No. 1, Jan. 2004, pp. 26–34.
16. Abdol-Hamid, K. S., Pao, S. P., Massey, S. J., and Elmiligui, A., "Temperature Corrected Turbulence Model for High Temperature Jet Flow," *Journal of Fluids Engineering*, Vol. 126, No. 5, 2004, pp. 844–850.
17. Morris, C. I. and Luke, E. A., "Implicit Large-Eddy Simulations of Hot and Cold Supersonic Jets in Loci-CHEM," AIAA Paper 2020-1333, Jan. 2020.
18. Georgiadis, N. J., Wernet, M. P., Locke, R. J., and Eck, D. G., "Mach Number and Heating Effects on Turbulent Supersonic Jets," *AIAA Journal*, Vol. 62, No. 1, Jan. 2024.
19. Wernet, M. P., Georgiadis, N. J., and Locke, R. J., "Raman Temperature and Density Measurements in Supersonic Jets," *Experiments. In Fluids*, Vol. 62, No. 3, 2021, pp. 1-21.
20. Wernet, M. P., Georgiadis, N. J., and Locke, R. J., "Velocity, Temperature and Density Measurements in Supersonic Jets," NASA/TM-20205007269 and AIAA Paper 2021-0596, Oct. 2020.
21. Georgiadis, N. J., Wernet, M. P., Winkler, C.M., Benton, S.I., and Connolly, B.J., "Summary of the 6th Propulsion Aerodynamics Workshop Nozzle Test Case: Heated Supersonic Axisymmetric Jets," AIAA Paper 2024-0749, Jan. 2024.
22. Pointwise, Version 18.3 Release 1 [Software]. 2021. URL: https://www.pointwise.com/
23. Zore, K., Aliaga, C., Selva, J., Zori, L., Makarov, B., "High-Fidelity SBES Simulations for Supersonic Nozzle Flows, AIAA Paper 2024-0753, Jan. 2024.
24. Birch, S. F., Lyubimov, D. A., Maslov, V. P., Secundov, A. N., and Yakubovsky, K. Y., "A RANS Based Jet Noise Prediction Procedure," AIAA Paper 2007-3727, June 2007.
25. Yoder, D.A., "Wind-US User's Guide," NASA TM2016-210145, Sept. 2016.
26. Biedron, R. T., Carlson, J. R., Derlaga, J. M., Gnoffo, P. A., Hammond, D. P., Jones, W. T., Kleb, B., Lee-Rausch, E. M., Nielsen, E. J., Park, M. A., Rumsey, C. L., Thomas, J.L., and Wood, W. A., "FUN3D User's Manual Version 13.3," NASA/TM 2018-219808, Feb. 2018.
27. Baurle, R. A., White, J.A ., Drozda, T. G., and Norris, A. T., "VULCAN-CFD Theory Manual: Ver. 7.2.0,: NASA TM 2022-000-8776, Nov. 2022.
28. Menter, F. R., "Improved Two Equation k-ω Turbulence Models for Aerodynamic Flows," NASA/TM 103975, Oct. 1992.
29. Menter, F. R., "Two Equation Eddy-Viscosity Turbulence Models for Engineering Applications," *AIAA Journal*, Vol. 32, No. 8, 1994, pp. 1598-1605.
30. Wilcox, D. C., Turbulence Modeling for CFD, 3rd edition, DCW Industries, Inc., La Canada CA, 2006.

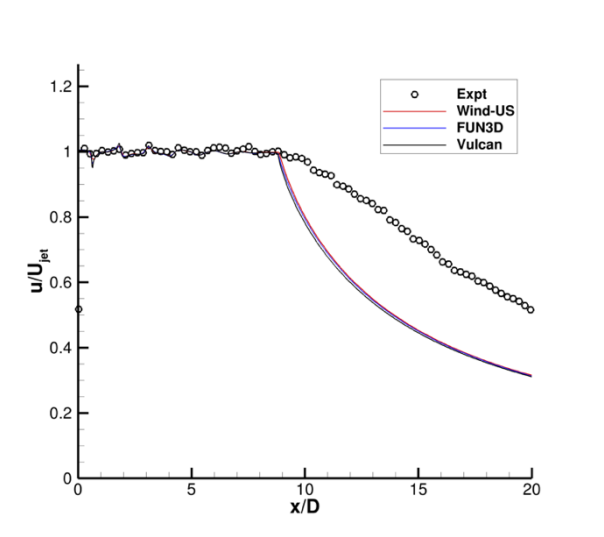

Fig. 2.— Centerline velocity comparisons for the temperature matched case.

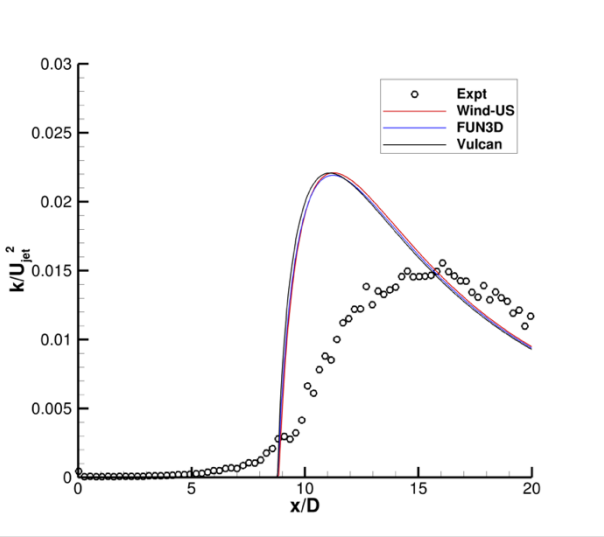

Fig. 3.— Centerline turbulent kinetic energy comparisons for the temperature matched case.

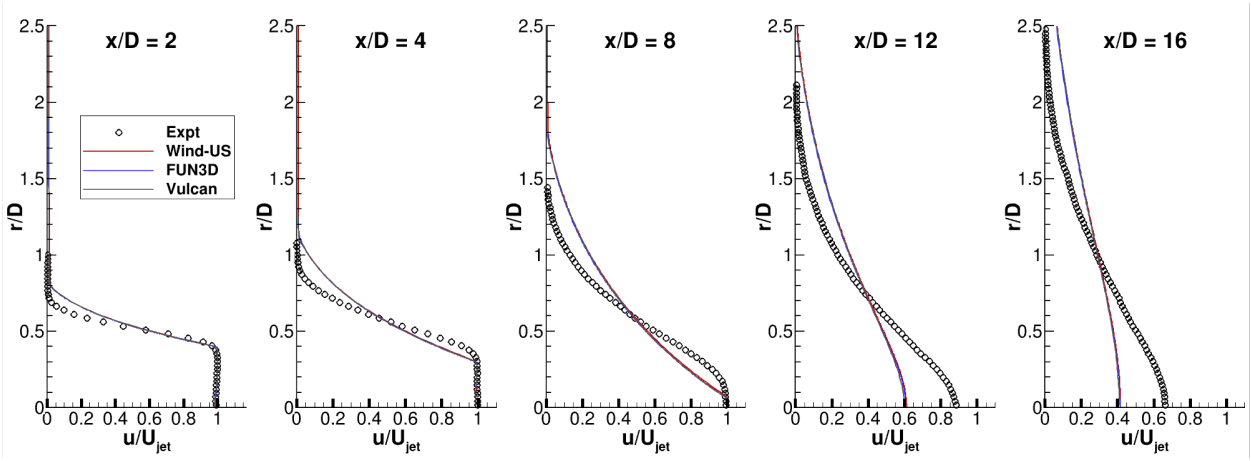

(a) Axial velocity

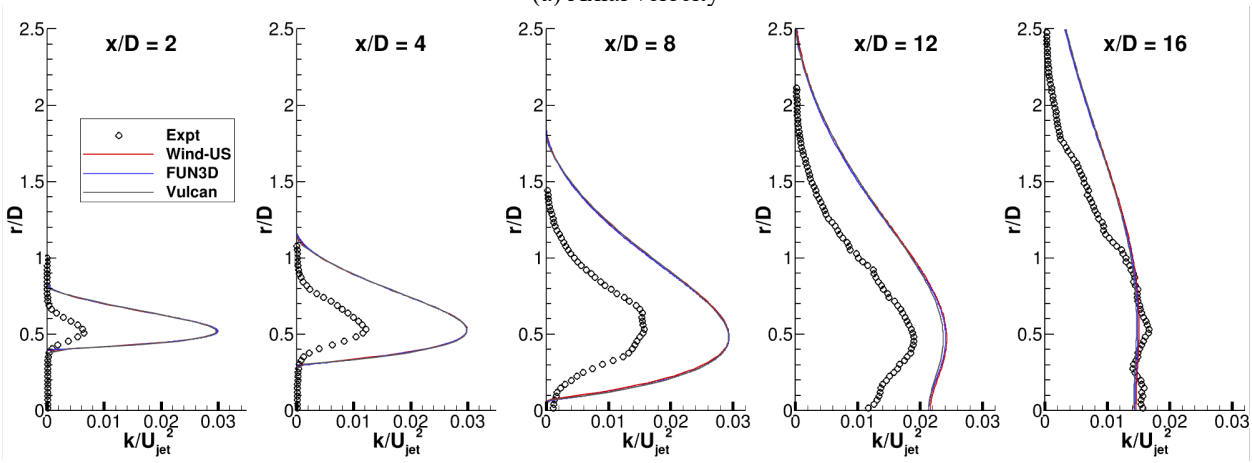

(b) Turbulent kinetic energy

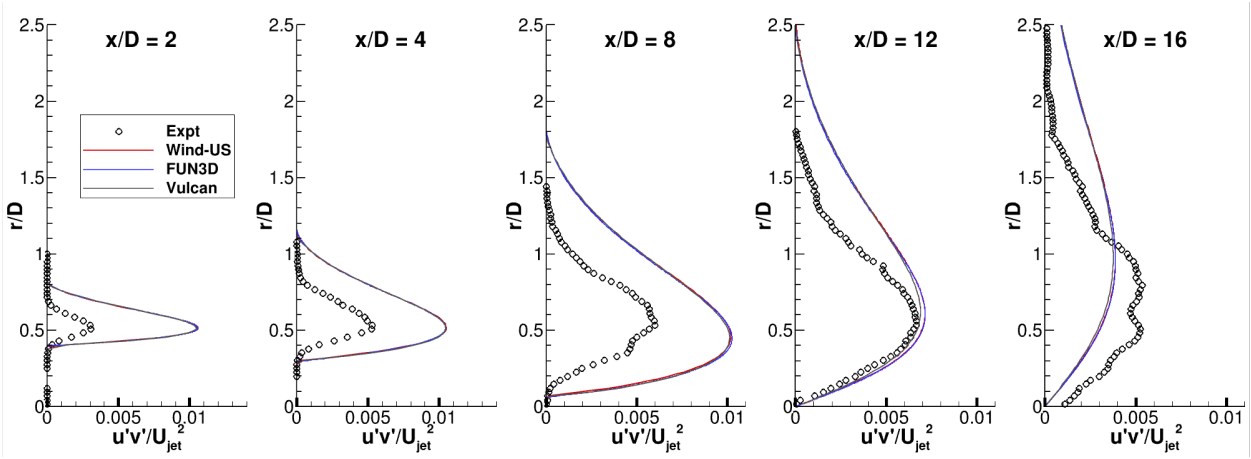

(c) Turbulent shear stress

Fig. 4.— Axial profiles of flow quantities for the temperature matched case.

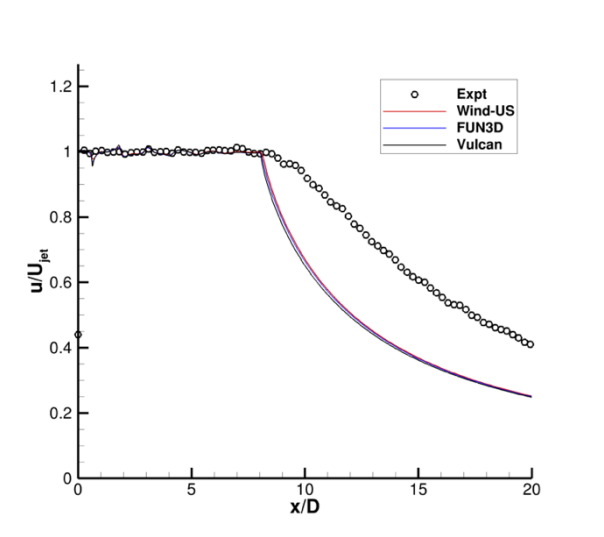

Fig. 5.— Centerline velocity comparisons for the heated Mach 1.63 jet case.

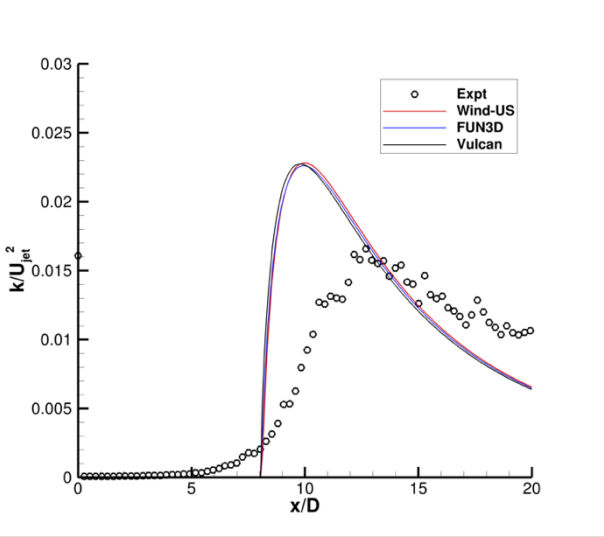

Fig. 6.— Centerline turbulent kinetic energy comparisons for the heated Mach 1.63 jet case.

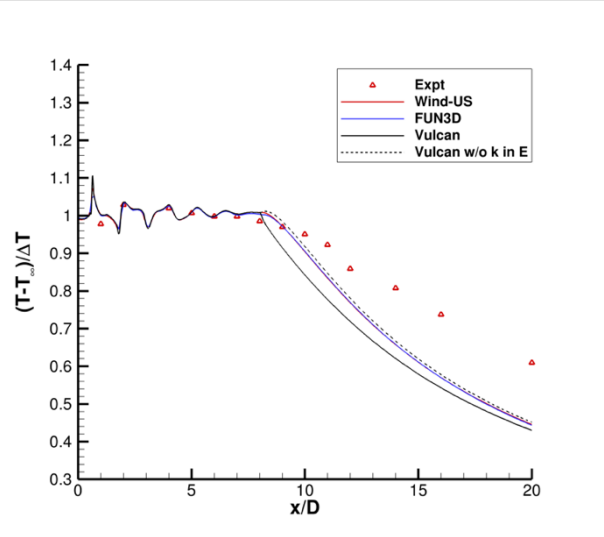

Fig. 7.— Centerline temperature comparisons for the heated Mach 1.63 jet case.

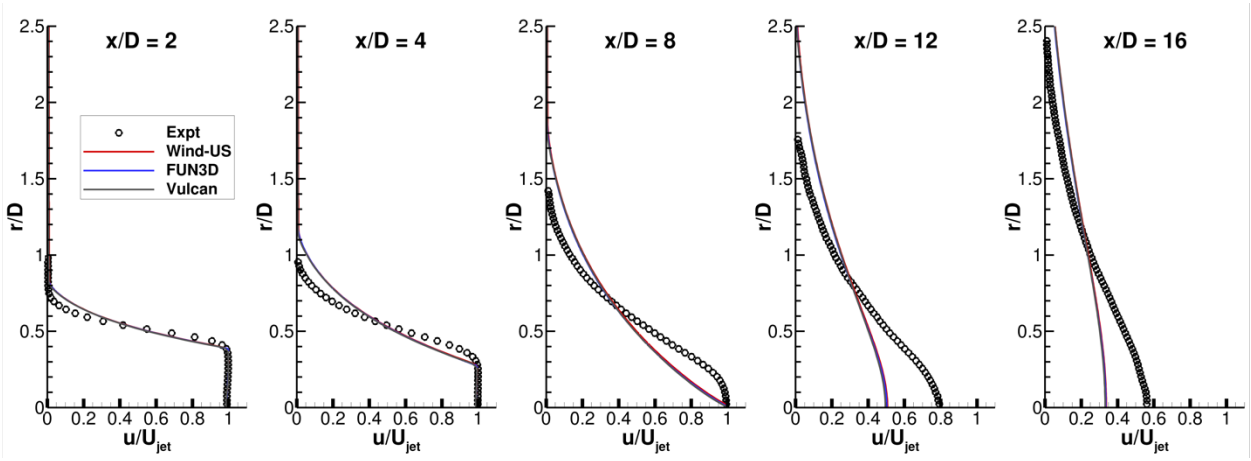

(a) Axial velocity

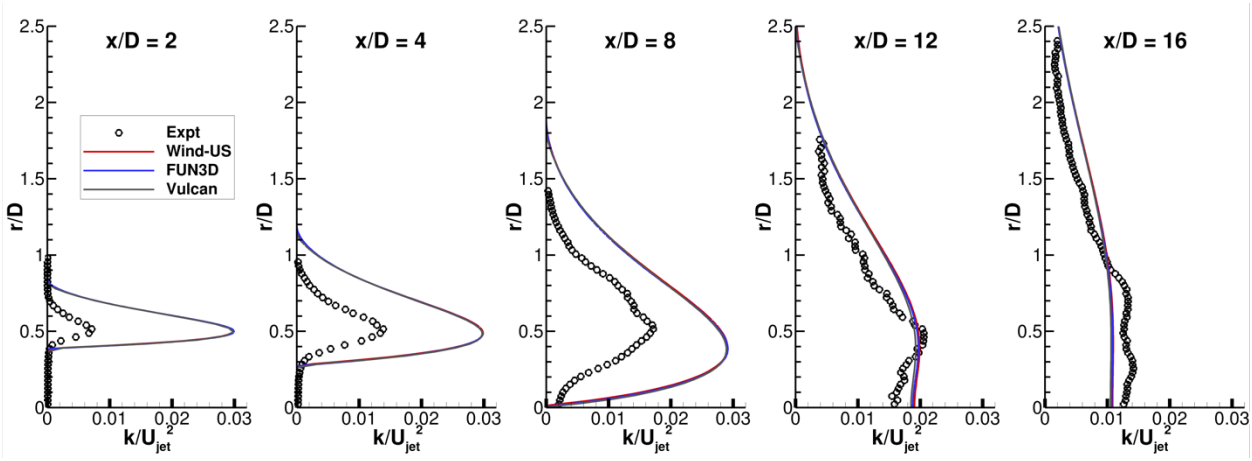

(b) Turbulent kinetic energy

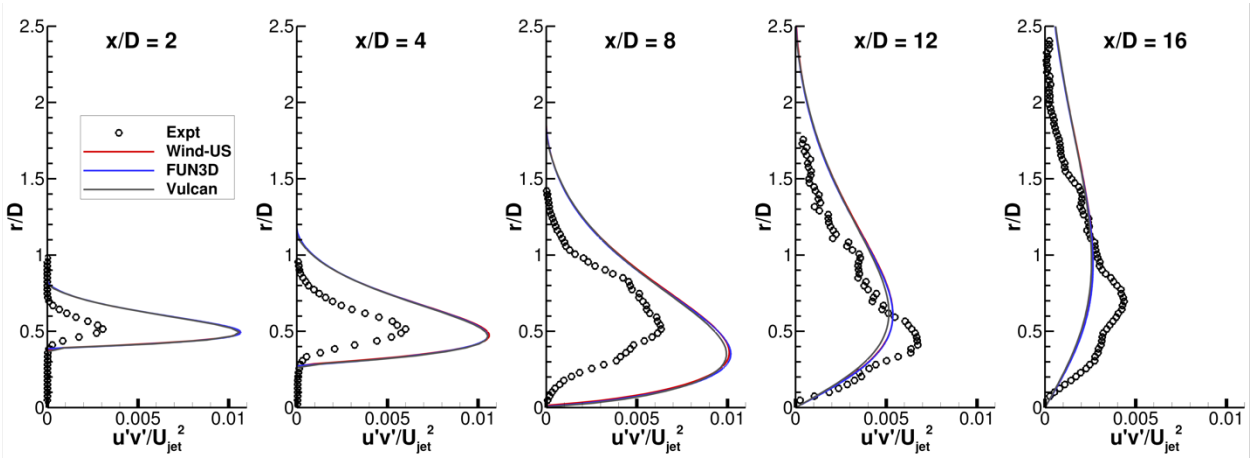

(c) Turbulent shear stress

Fig. 8.— Axial profiles of flow quantities for the heated jet case.

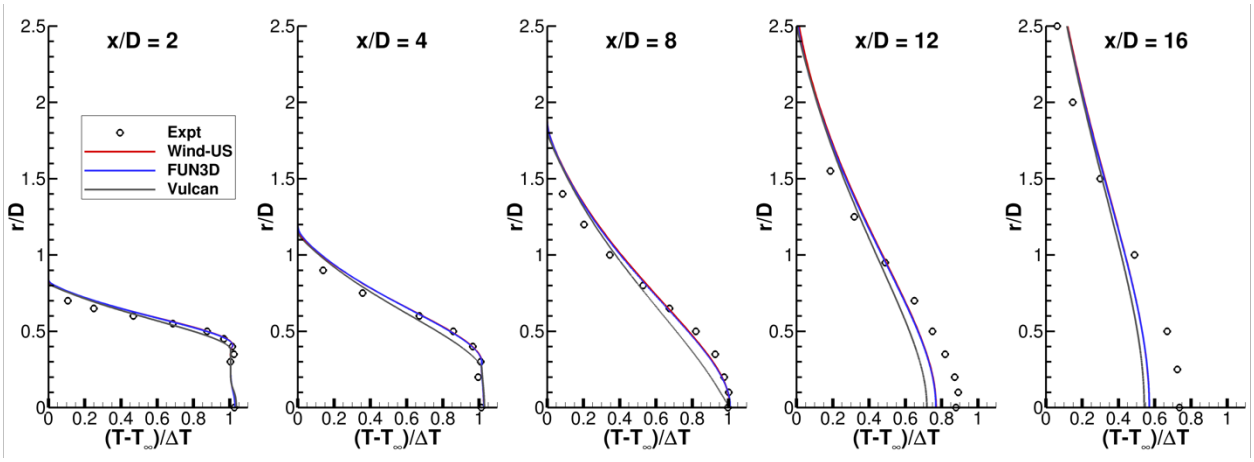

(a) Standard VULCAN-CFD result accounting for TKE in the energy equation

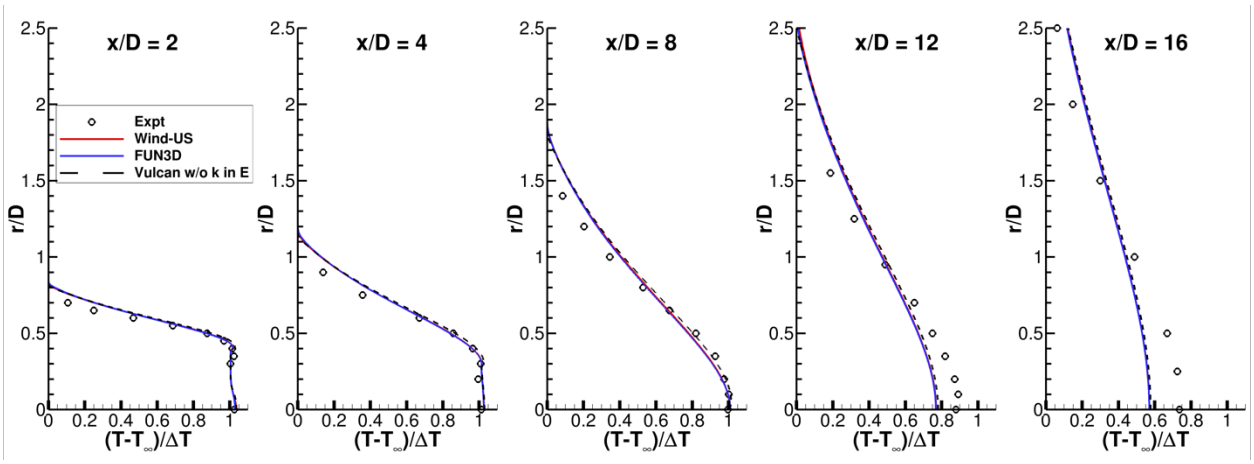

(b) Modified VULCAN-CFD result to ignore TKE in the energy equation

Fig. 9.— Static temperature comparisons for the heated jet case.

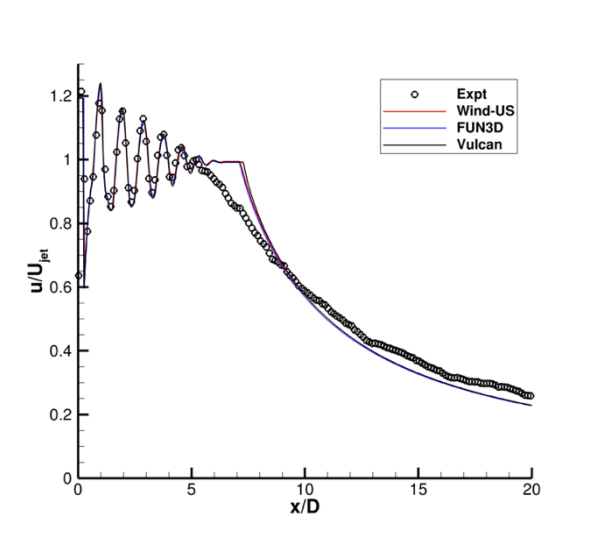

Fig. 10.— Centerline velocity comparisons for the off-design Mach 1.63 jet case.

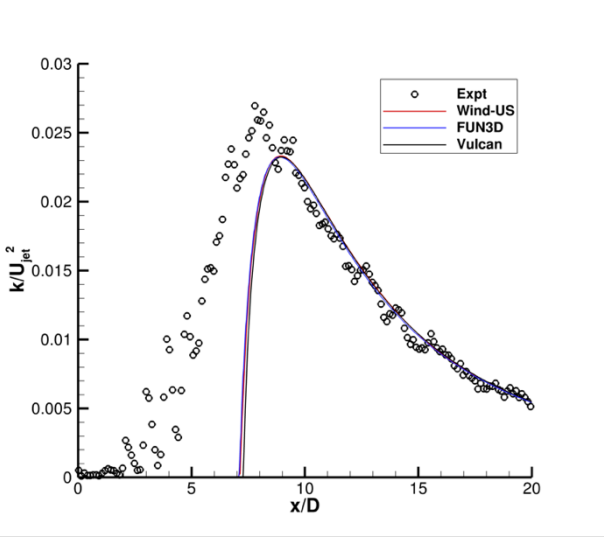

Fig. 11.— Centerline turbulent kinetic energy comparisons for the off-design Mach 1.63 jet case.

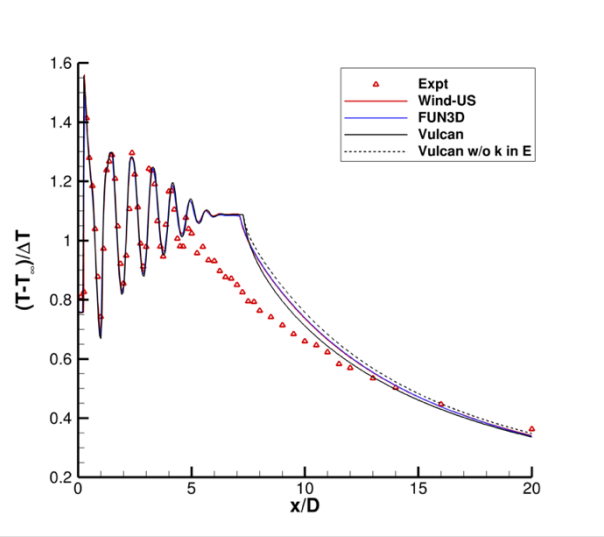

Fig. 12.— Centerline temperature comparisons for the off-design Mach 1.63 jet case.

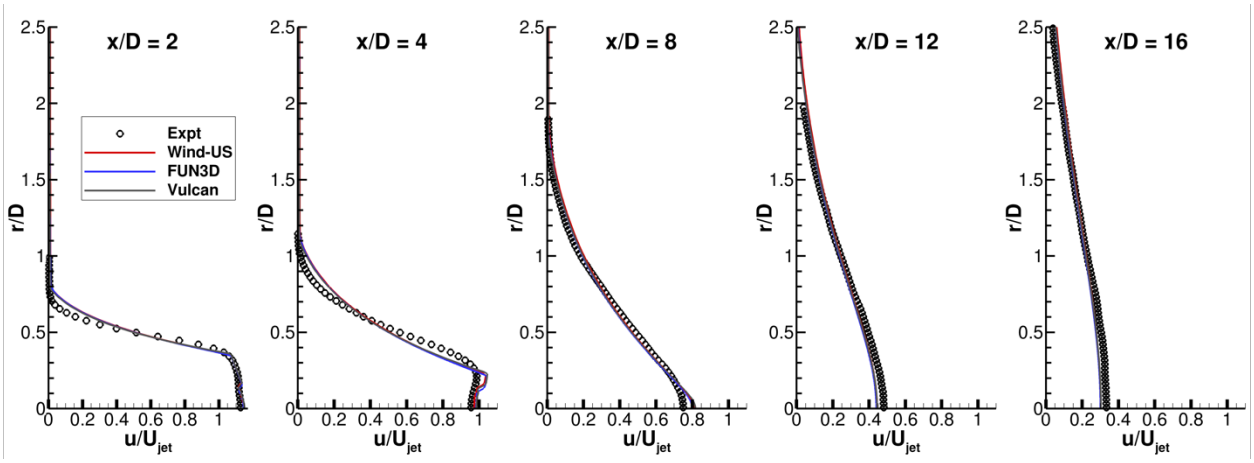

(a) Axial velocity

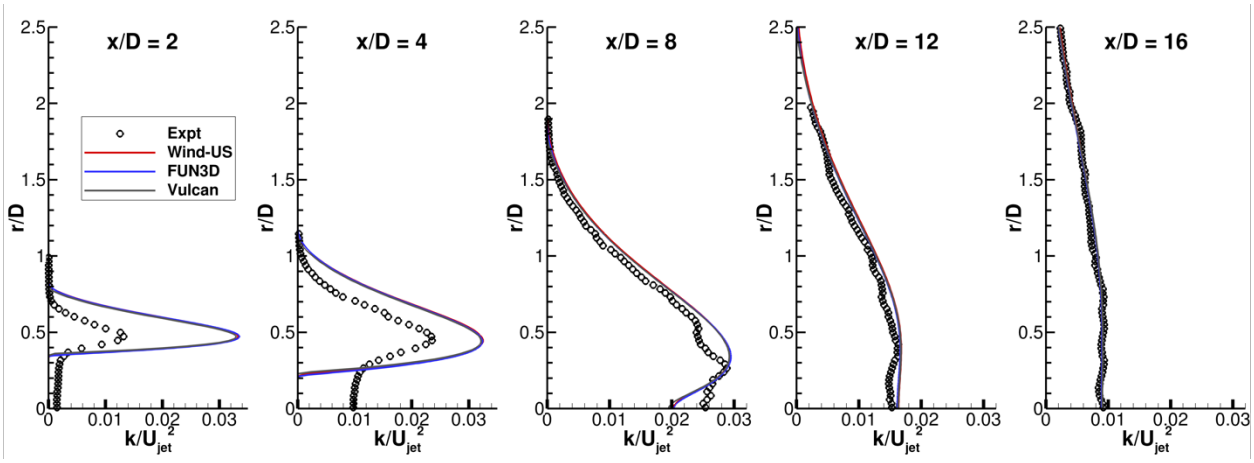

(b) Turbulent kinetic energy

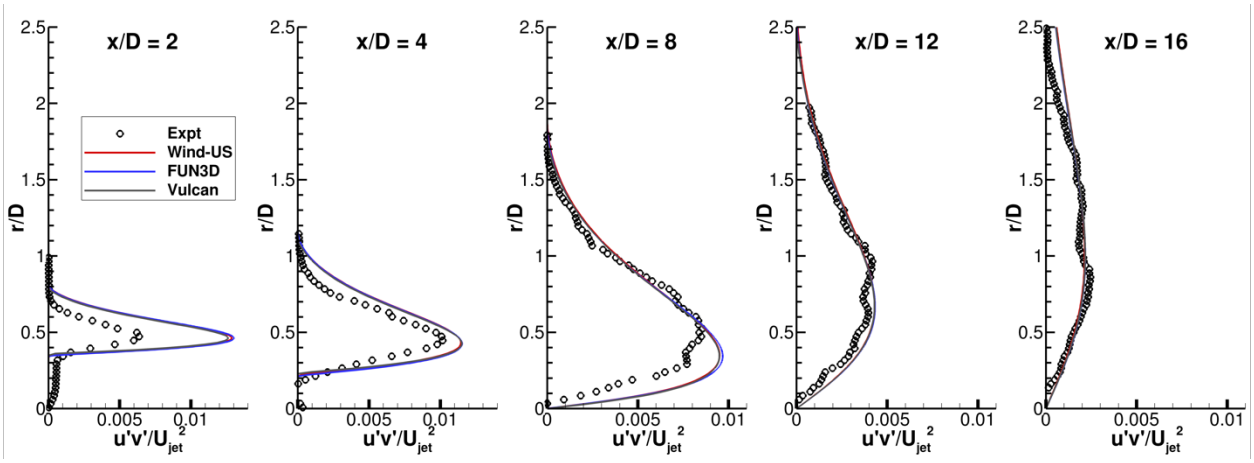

(c) Turbulent shear stress

Fig. 13.— Axial profiles of flow quantities for the off-design jet case.

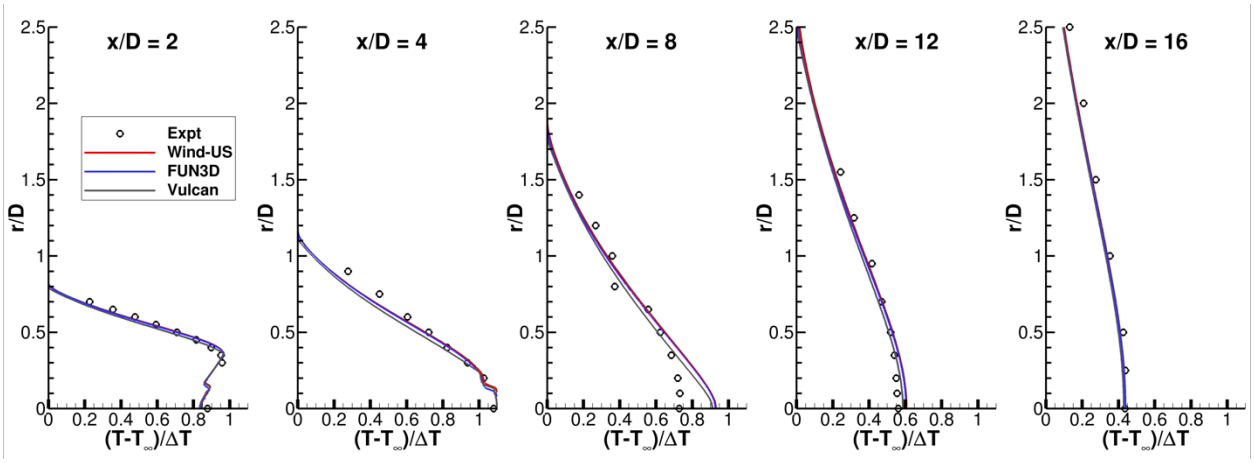

(a) Standard VULCAN-CFD result accounting for TKE in the energy equation

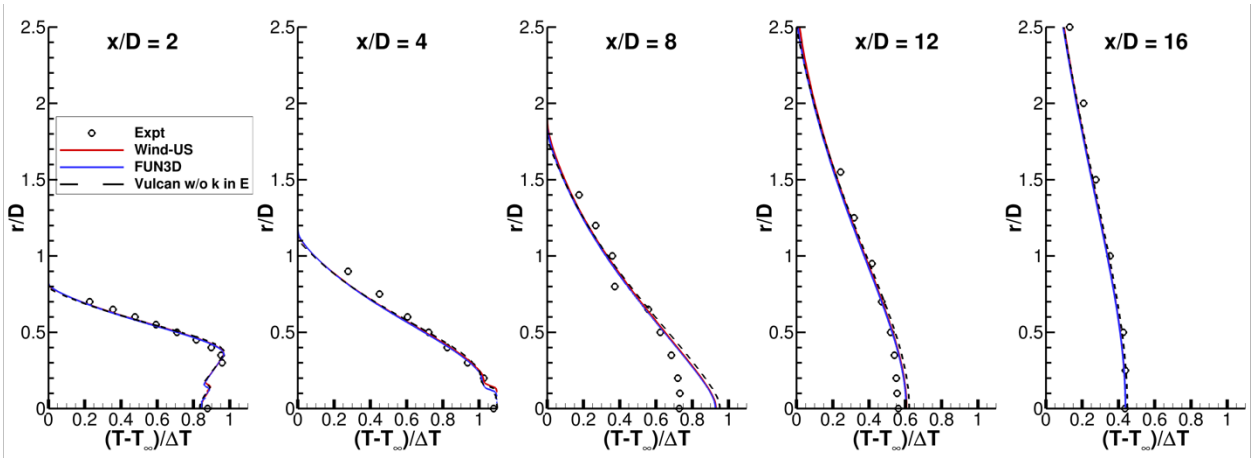

(b) Modified VULCAN-CFD result to ignore TKE in the energy equation

Fig. 14.— Static temperature comparisons for the off-design jet case.

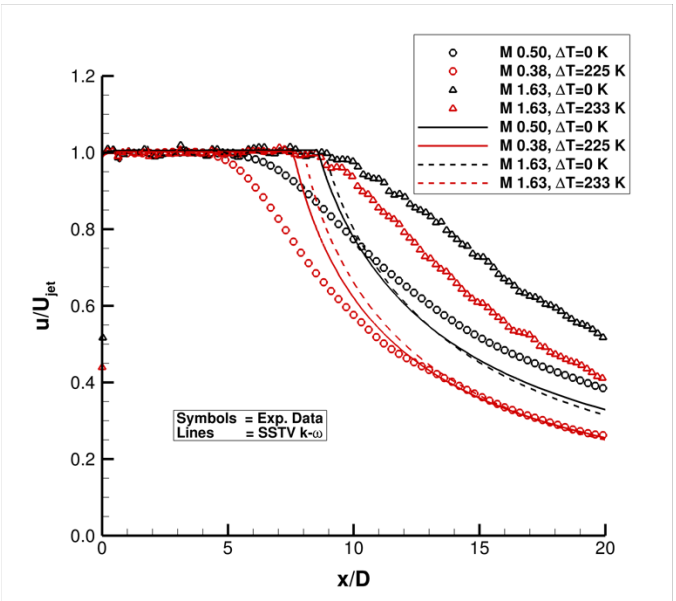

(a) Axial velocity

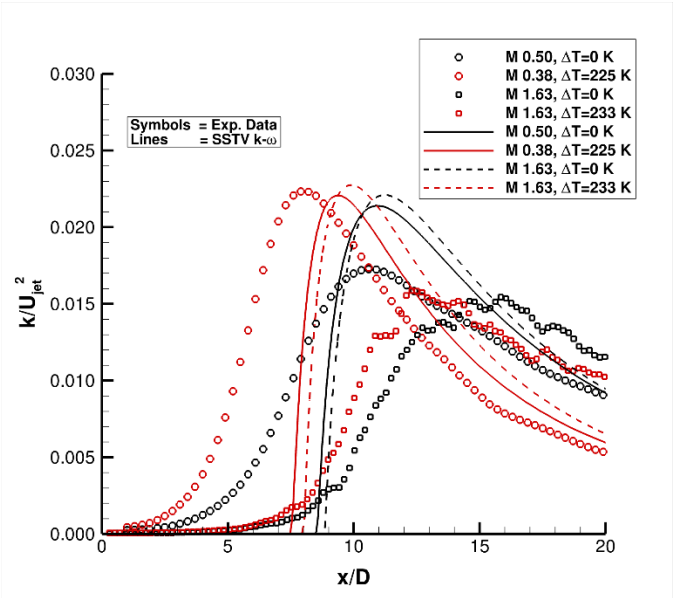

(b) Turbulent kinetic energy

Fig. 15.— Comparison of subsonic and supersonic round jets.